OPEN ACCESS

Original research

Single-cell multimodal analysis reveals the dynamic immunopathogenesis of HBV-ACLF progression

Xi Liang,[1] Jinjin Luo,[1] Qian Zhou,[1] Jiaojiao Xin,[1] Jiaqi Li,[2] Bo Peng,[3,4] Meiqian Hu,[1] Jing Jiang,[1] Wei Qiang,[1] Peng Li ,[5] Pengcheng Chen,[6] Heng Yao,[1,7] Huafen Zhang,[1] Xingping Zhou,[1] Jiaxian Chen,[1] Wen Hu,[1] Bingqi Li,[1] Shiwen Ma,[1] Xiao Wu,[1] Xiao Li,[1] Jing Zhang,[1] Jinlin Cheng,[1] Shourong Liu,[8] Xiaoqing Fu,[8] Yingyan Lu,[9] Yingzi Ming,[3,4] Xin Chen,[10,11] Dongyan Shi,[1] Jun Li [1]

► Additional supplemental material is published online only. To view, please visit the journal online (https://doi.org/10.1136/gutjnl-2024-333308).

For numbered affiliations see end of article.

Correspondence to
Professor Jun Li;
lijun2009@zju.edu.cn
Dr Dongyan Shi;
shidongyan@zju.edu.cn
Professor Xin Chen;
xinchen@zju.edu.cn and
Professor Yingzi Ming;
mingyz_china@csu.edu.cn

XL, JL, QZ, JX, JL and BP contributed equally.

Received 9 July 2024
Accepted 25 July 2025
Published Online First 21 August 2025

Watch Video
https://gut.bmj.com/

Check for updates

To cite: Liang X, Luo J, Zhou Q, *et al*. *Gut* 2026;**75**:367–381.

ABSTRACT

Background Acute-on-chronic liver failure (ACLF) is a life-threatening syndrome involving dysfunction of multiple immune cell types.

Objective This study aimed to comprehensively depict the dynamic trajectory of immune responses throughout the disease course of HBV-related ACLF (HBV-ACLF).

Design Single-cell RNA sequencing and single-cell proteomics were performed on the peripheral blood mononuclear cells of 45 samples from 17 patients who were hospitalised (progressive/stable/recovering course of HBV-ACLF, 6/5/6) and 15 control subjects (liver cirrhosis, chronic hepatitis B and healthy controls, 5/5/5). Functional and mechanistic experiments were validated in vivo and in vitro.

Results Single-cell multiomics analysis revealed specific changes in the peripheral immune response in ACLF. $VCAN^{+}CD14^{+}$-monocytes with activated interferon-stimulated genes and enhanced inflammatory functions, stimulated by HBV relapse and expanded in ACLF-1, fuelling early inflammatory storm. The subsequent apoptotic hepatocytes predominantly induce hyperinflammatory C-X-C motif chemokine receptor 2 $(CXCR2)^{+}$-neutrophils and $CD163^{+}$-monocytes, enriching in patients with progressive ACLF and serving as significant markers of disease deterioration. Cytotoxic T-cells were functionally impaired and significantly decreased in progressive patients. $CXCR2^{+}$-neutrophils exhibited immunosuppressive activity and induced the exhaustion of cytotoxic T-cells. Pharmacological inhibition of CXCR2 significantly reduced neutrophils infiltration, restored cytotoxic T-cells and showed therapeutic effect in ACLF mice. Six immune cellular modules (CMs) were identified for patient stratification, with CM2 and CM6 showing strong predictive value for disease outcomes, and CM3 indicating a potential early therapeutic window.

Conclusion Our longitudinal multiomics study revealed the dynamic evolution of the immune response in HBV-ACLF and characterised diverse immune patterns for the future precise management and therapeutic intervention.

WHAT IS ALREADY KNOWN ON THIS TOPIC

⇒ Acute-on-chronic liver failure (ACLF) is a critical syndrome with high short-term mortality. The course of ACLF is highly dynamic, with potential for rapid progression shortly after admission.
⇒ The dynamics of immune changes that contribute to the development and progression of ACLF remain unclear.
⇒ Longitudinal single-cell multimodal analysis of molecular mechanism underlying the pathophysiology of HBV-related ACLF (HBV-ACLF) is still lacking.

WHAT THIS STUDY ADDS

⇒ This study provides a comprehensive view of the dynamic immune response during HBV-ACLF progression at single-cell resolution.
⇒ The collaborative crosstalk of the innate and adaptive immune system was delineated, highlighting the roles of $VCAN^{+}CD14^{+}$ monocytes in the early-stage inflammatory response, C-X-C motif chemokine receptor 2 $(CXCR2)^{+}$ neutrophils and $CD163^{+}$ monocytes in disease deterioration and cytotoxic T cells in disease recovery.
⇒ Six immune patterns were identified that stratify immune responses during the progression of HBV-ACLF, with the specific immune patterns cellular modules (CM)2 and CM6 correlating with disease outcomes, while CM3 could serve as an early therapeutic window.

HOW THIS STUDY MIGHT AFFECT RESEARCH, PRACTICE OR POLICY

⇒ Single-cell multimodal atlas from longitudinal sampling could be a valuable resource for obtaining a deeper understanding of the peripheral immune system in HBV-ACLF.
⇒ The identification of specific immune subsets that drive distinct stages of HBV-ACLF lays the groundwork for the development of therapeutic strategies aimed at optimising the immune environment in HBV-ACLF.
⇒ The stratified immune patterns serve as a tool for identifying disease states and guiding personalised treatment interventions.

INTRODUCTION

Acute-on-chronic liver failure (ACLF) is a critical syndrome characterised by hepatic or extrahepatic organ failure with high short-term mortality that

develops in patients with advanced chronic liver disease regardless of cirrhosis.[1] The course of ACLF is highly dynamic, with potential for recovery, stability or progression shortly after admission.[2] Few effective treatments exist for ACLF, with liver transplantation being an effective option limited by organ shortages.[3] Understanding the dynamic molecular mechanisms and immune responses in ACLF is critical for developing prognostic tools, targeted therapeutic interventions and personalised medicine approaches.

The Chronic Liver Failure (CLIF) Consortium acute-on-chronic liver failure in cirrhosis (CANONIC) study identified intense systemic inflammation and mitochondrial metabolic dysfunction, triggered by proinflammatory precipitants like alcohol-related hepatitis and bacterial infection, as key drivers of ACLF development from acutely decompensated cirrhosis (ADC).[4 5] The PREDICTing Acute-on-Chronic Liver Failure (PREDICT) study identified precipitants that are significantly associated with a distinct clinical course of ADC.[6] Our recent Chinese Group on the Study of Severe Hepatitis B (COSSH) study highlighted hepatotropic viral infections, such as HBV reactivation, as the most common trigger of ACLF in Asia.[1] Innate immune activation and adaptive immune suppression with subsequent metabolic disruption are central to HBV-related ACLF (HBV-ACLF) pathogenesis, resembling that of alcoholic liver disease-related ACLF (ALD-ACLF).[7]

Previous studies have shown that immune dysregulation is pivotal in ALD-ACLF and HBV-ACLF, primarily through cross-sectional designs and single-omics methods.[4 7 8] A longitudinal analysis of immune cell dynamics is needed to uncover the pathological mechanisms driving disease progression. Single-cell technology approaches, including single-cell mRNA sequencing (scRNA-seq) and single-cell proteomics (cytometry by time of flight, CyTOF), are powerful tools for characterising immune responses at the cellular level. This study employed longitudinal single-cell multiomics to study the dynamic trajectories of the innate and adaptive immune responses in HBV-ACLF and explored the molecular mechanisms underpinning disease progression. Cross-sectional analysis was performed to capture cellular changes and gene expression during early disease stages, given the challenge of obtaining early-stage samples from progressing patients.

METHODS

Study design

To elucidate the dynamic immune response of HBV-ACLF, we collected 45 peripheral blood mononuclear cell (PBMC) samples from 17 patients who were hospitalised and 15 controls for scRNA-seq and CyTOF (figure 1A). PBMCs from each patient were collected at initial admission (T1, within 24 hours) and at a second time (T2, within 2 weeks) of hospitalisation when the patients were still symptomatic. Among the patients, six were in the progressive stage of ACLF, five in the stable stage and six in the recovering stage. Four patients had a single sample, as their second samples did not meet cell capture quality check criteria and were excluded from this study. Controls included five healthy controls (HCs), five individuals with chronic hepatitis B (CHB) and five individuals with liver cirrhosis (LC), representing different stages of ACLF development. Validation cohorts were additionally enrolled to confirm the robustness of findings. scRNA-seq analysis from 11 liver tissue samples (HBV-ACLF, n=5; LC, n=3; HC, n=3), 13 PBMC samples from six patients with non-HBV-ACLF and publicly available sepsis data (GSE151263)[9] were used to evaluate the generalisability and liver-specificity of the immune cell dynamics. Bulk RNA-seq of PBMCs from 178 subjects (HBV-ACLF, n=135; non-ACLF, n=10; LC, n=9; CHB, n=10; HC, n=14), 67 patients with non-HBV-ACLF and 31 sepsis patients were used to support the identification of key immune cell subsets and clinical application of associated gene signatures. Specific cell types were verified in 19 subjects (HBV-ACLF, n=11; non-ACLF, n=5; HC, n=3) using flow cytometry. Patients with ACLF in each cohort were enrolled using stratified random sampling based on the prevalence of ACLF grades. Antiviral nucleoside analogues were immediately administered to patients if HBV DNA was detected according to the Consensus Recommendations of the Asian Pacific Association for the Study of the Liver (2009).[10] Functional and mechanistic experiments were validated in vivo and in vitro.

Detailed materials and methods, including patient with HBV-ACLF's clinical information, ACLF prognostic scores, the experimental procedures and data analysis of scRNA-seq, CyTOF and bulk RNA-seq, are provided in the online supplemental Methods.

Patient and public involvement

Patients were not involved in the development of the research question and outcome measures.

RESULTS

Single-cell immune landscape of PBMCs in HBV-ACLF

To better understand the pathogenesis of ACLF development and progression, we performed joint scRNA-seq and CyTOF analyses of 45 PBMC samples from 32 subjects, including ACLF, non-ACLF, LC, CHB and HC groups (figure 1A). Patients were defined as having progressive, stable or recovering ACLF based on prognosis. Clinical characteristics are provided in online supplemental Table 1 and figure 1. There were no significant differences in precipitants among the groups. Progressive patients had higher international normalised ratio (INR), total bilirubin (TB), creatinine and neutrophil-to-lymphocyte ratio than stable and recovering patients, along with more frequent organ failure.

After quality control, we obtained 379 132 high-quality single cells from 45 samples. Five major cell clusters ($CD4^+$ T, $CD8^+$ T, natural killer (NK), B and myeloid cells) were identified by canonical marker expression (figure 1B and C and online supplemental figure 2). We identified 15 T-cell, 7 NK-cell, 6 B-cell and 13 myeloid-cell subclusters (figure 1B and online supplemental Table 2). These clusters showed differential enrichment by disease stage and course (figure 1D and online supplemental figure 2B). Myeloid cells were more enriched in ACLF, especially in progressive patients (figure 1E). Global gene expression analysis revealed the most pronounced dysregulation in myeloid cells of progressive patients, while T and NK cells showed changes in recovering patients (figure 1F). Cellular deconvolution analysis using bulk transcriptome data with CIBERSORTx confirmed increased myeloid cells and decreased T and NK cells with ACLF progression (online supplemental figure 2C).

CyTOF analysis of the same samples identified five major immune clusters at the single-cell protein level (online supplemental figure 3A and B, Table 3). These results were consistent with the transcriptomic data (online supplemental figure 3C), highlighting distinct immune characteristics for each ACLF stage and disease course.

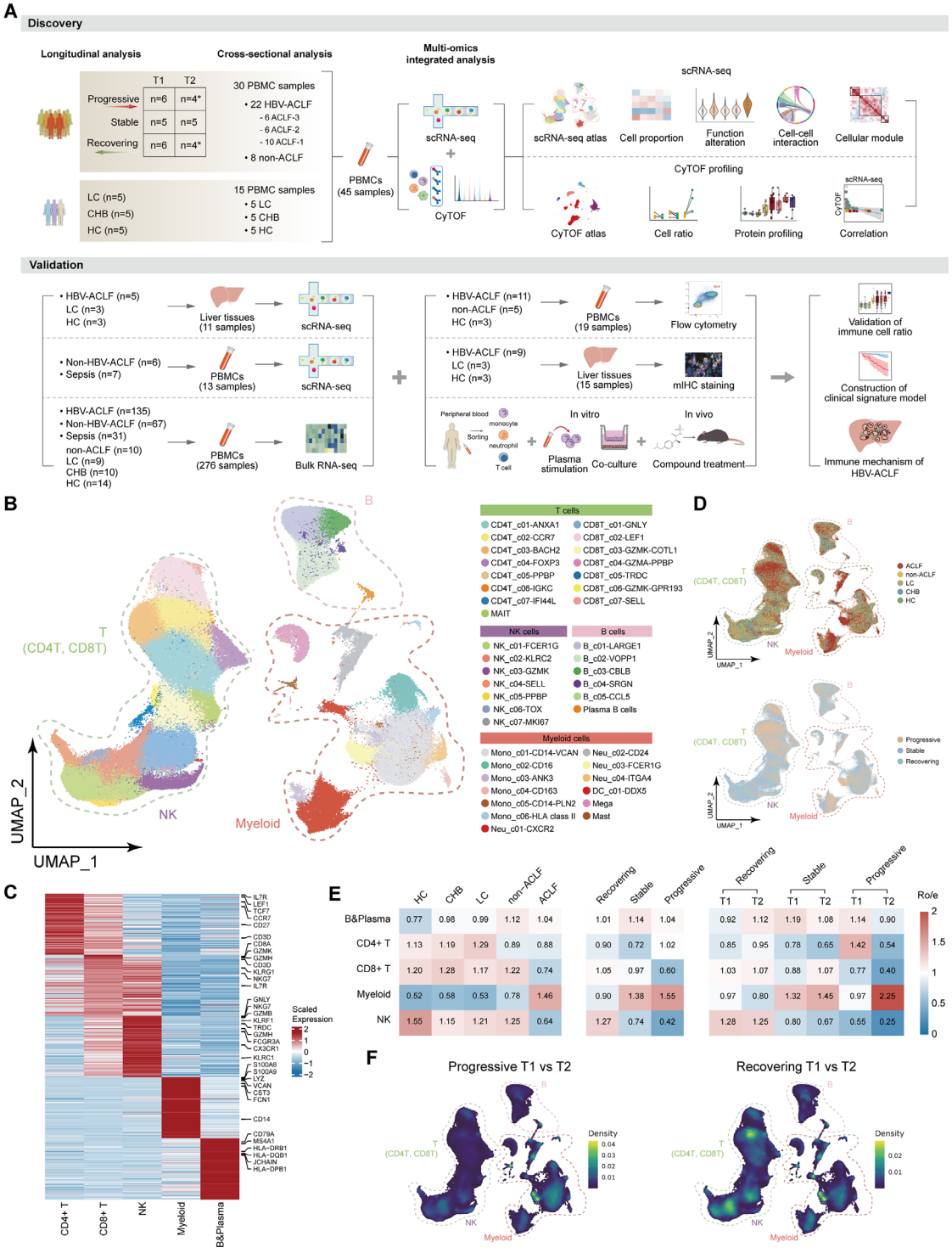

Figure 1 Single-cell transcriptome map of patients with HBV-ACLF. (A) Schematic diagram of the study design. 30 PBMC samples from 17 patients who were hospitalised with HBV-ACLF and patients with early-stage non-ACLF, as well as 15 control subjects, were included in the discovery cohort. PBMC samples were collected at two time points for all patients, except for four patients for whom only a single sample was available (*). scRNA-seq and CyTOF were jointly performed. Validation cohorts included scRNA-seq analysis of 11 liver tissue samples from five HBV-ACLF, three patients with LC and HC, as well as 13 PBMC samples from six non-HBV-ACLF and seven patients with sepsis, bulk RNA-seq analysis of 276 subjects, comprising 135 patients with HBV-ACLF, 67 patients without HBV-ACLF and 31 patients with sepsis. (B) UMAP plot of the 379 132 cells from 45 PBMC samples, including 4 major clusters and 41 subclusters. (C) Gene expression heatmap for each major cluster. (D) UMAP plot showing disease severity (upper) and course (lower) distributions. (E) Group preference of each major cluster measured by the ratio of observed to randomly expected cell numbers (Ro/e). (F) Kernel density estimates of molecular response magnitude in patients with progressive (left) and recovering (right) ACLF at T2 versus T1. ACLF, acute-on-chronic liver failure; CHB, chronic hepatitis B; CyTOF, cytometry by time of flight; HBV-ACLF, HBV-related ACLF; HC, healthy control; LC, liver cirrhosis; MAIT, mucosal-associated invariant T; mIHC, multiplex immunohistochemistry; NK, natural killer; PBMC, peripheral blood mononuclear cell; scRNA-seq, single-cell RNA sequencing; UMAP, uniform manifold approximation and projection; T1, sample collected at initial admission (within 24 hours); T2, sample collected the second time (within 2 weeks).

Dynamic myeloid cell subset alterations in ACLF severity and progression

We first investigated myeloid cell heterogeneity given their predominance in ACLF. 13 myeloid cell clusters with distinct gene signatures were identified by unsupervised clustering (figure 2A–B). Among these, six subsets were characterised as monocytes, including Mono_c01-CD14-VCAN, Mono_c02-CD16, Mono_c03-ANK3, Mono_c04-CD163, Mono_c05-CD14-PLIN2 and Mono_c06-HLA class II (online supplemental figure 4A-C). Functional enrichment analysis of immunology pathways revealed enhanced inflammatory response and activation/cytokine signalling of monocytes during the early stage of ACLF, especially in ACLF-1, but decreased in ACLF-3 and progressive ACLF (figure 2C, online supplemental Table 4).

Monocyte composition varied among disease groups (online supplemental figure 4D). The proportion of Mono_c01-CD14-VCAN increased in ACLF-1/2 but significantly decreased in ACLF-3, while Mono_c04-CD163 significantly increased in ACLF-3 (figure 2D). Immune cell trajectory analysis revealed that progressive patients exhibited distinct immune response trajectories characterised by a significant increase in Mono_c04-CD163 at T2 (figure 2D). Mono_c04-CD163 proportions were positively correlated with prognostic scores (COSSH-ACLFs and CLIF-C ACLFs) (online supplemental figure 4E). Myeloid cell subsets were further analysed with CyTOF, revealing increased classical monocytes and $CD163^+$ monocytes in patients with ACLF (figure 2E). Correlation analysis showed the cell composition dynamics of CyTOF dataset were in good agreement with scRNA-seq results (figure 2F).

Notably, interferon gamma response, type I interferon response and the inflammatory response were elevated in ACLF-1 but reduced in ACLF-2 within Mono_c01-CD14-VCAN (figure 2G). Differential expression analysis showed that interferon-stimulated genes (IFITM3, IF44L, IFI6) and inflammatory-related genes (S100A8, S100A9, S100A12) were upregulated in ACLF-1 but downregulated in ACLF-2 (figure 2H). Transcription factor regulon analysis revealed high activity of interferon regulatory factors (IRF5 and IRF7) in Mono_c01-CD14-VCAN (figure 2I). These findings suggest that the expansion of activated, proinflammatory Mono_c01-CD14-VCAN corresponds to viral replication in the early stage of ACLF, particularly ACLF-1. Mono_c04-CD163 cells, based on M1/M2-specific signature genes (online supplemental Table 5), were associated with the CD39 signalling network in progressive ACLF, indicating a strong anti-inflammatory effect (online supplemental figure 4F and G).

Collectively, these findings highlight the role of $VCAN^+CD14^+$ monocytes in the early stage of ACLF following HBV relapse and suggest that dynamic changes in $CD163^+$ monocytes with an anti-inflammatory phenotype are associated with ACLF severity, especially in the end stage.

Low-density neutrophils massively emerge in the end-stage of ACLF

An anti-inflammatory immune phenotype emerged in severe ACLF, whereas monocyte-mediated inflammation declined in ACLF-3 (figure 2C). Using neutrophil gene markers,[11–13] we identified four distinct low-density neutrophil (LDN) clusters in PBMC samples (figure 2A). LDNs were absent in control groups but prevalent in patients with ACLF (online supplemental figure 5A). LDNs showed elevated inflammatory response, activation/cytokine signalling and energy metabolism in ACLF-3, especially in progressive patients at T2 (figure 2C). The four LDN clusters included mature neutrophils (Neu_c01-CXCR2, Neu_c03-FCER1G), pro-neutrophils (Neu_c02-CD24) and preneutrophils (Neu_c04-ITGA4) (online supplemental figure 5B-D). Pseudotime and RNA velocity analyses revealed potential developmental transitions of neutrophil clusters from pro-neutrophils (Neu_c02-CD24) through preneutrophils (Neu_c04-ITGA4) to mature neutrophils (Neu_c01-CXCR2, Neu_c03-FCER1G) (online supplemental figure 5E-H). The proportion of Neu_c01-CXCR2 significantly increased in ACLF, particularly in ACLF-3 (figure 2D). Trajectory analysis confirmed these specific phenotypes, with mature neutrophils being prevalent in ACLF (online supplemental figure 5G). Longitudinal analysis showed increased Neu_c01-CXCR2 in the end stage of progressive ACLF, positively correlated with prognostic scores (COSSH-ACLFs and CLIF-C ACLFs) (figure 2D, (online supplemental figure 5I). CyTOF analysis corroborated changes in LDN numbers aligned with scRNA-seq results (figure 2E,F).

Mature neutrophils, particularly Neu_c01-CXCR2, exhibited a hyperinflammatory phenotype (online supplemental figure 6A). Their activation elevated in progressive patients at T2, mirroring proportion changes (online supplemental figure 6B). Alarmins S100A8 and S100A9 were abundant across neutrophil subsets, with high levels of neutrophil extracellular traps genes (PADI4) and neutrophil activation/dysregulation (CD24, OLFM4, LCN2, BPI) in Neu_c02-CD24 (online supplemental figure 6C). Neu_c02-CD24 functions, including hypoxia, inflammatory response, tumour necrotic factor alpha (TNFa) signalling via nuclear factor kappa B (NFKB) and janus kinase/signal transducers and activators of transcription (JAK STAT) signalling pathways, were significantly elevated in ACLF-3 and progressive patients at T2 (online supplemental figure 6D and E). Cell–cell interactions between Neu_c01-CXCR2 and Mono_c04-CD163, both showing similar proportional changes in ACLF, were analysed via CellChat analysis (figure 2J). Crosstalk between these cells involved inflammatory-related signalling pathways (ADGRE5, ANNEXIN, VISFATIN and RESISTIN), with ligand-receptor interactions (ADGRE5-CD55, ANXA1-FPR1, NAMPT-INSR and RETN-CAP1) intensifying in progressive patients at T2.

Taken together, these findings suggest that dysfunctional neutrophils drive systemic inflammation in the end stage of ACLF, collaborating with anti-inflammatory $CD163^+$ monocytes and contributing to poor outcomes.

Validation of inflammatory activation of myeloid cell subsets in ACLF

Given the significant alterations in $VCAN^+CD14^+$ monocytes during the early stage of ACLF and C-X-C motif chemokine receptor 2 $(CXCR2)^+$ neutrophils and $CD163^+$ monocytes during disease progression, we validated the presence and functional characteristics of these immune subsets. Flow cytometry analysis confirmed increased $CD14^+CD163^-$ cells in the early stage of ACLF and $CD163^+IL1R2^+$ cells in patients with progressive ACLF (figure 3A,B). scRNA-seq analysis of liver tissues from patients with HC, LC and ACLF identified $CD163^+$ Kupffer cells, $CXCR2^+$ neutrophils and $VCAN^+$ monocytes, with $CD163^+$ Kupffer cells and $CXCR2^+$ neutrophils enriched in the livers of ACLF (figure 3C). And the expression of key genes in these subsets was significantly elevated in the liver of the ACLF rat model induced by injecting D-galactosamine and lipopolysaccharides into porcine serum-treated rats (PRJNA713912)[14] (online supplemental figure 7). Multiplex immunofluorescence staining confirmed an increase in $CXCR2^+$ neutrophils and $CD163^+$ macrophages in the livers of ACLF, with co-localisation

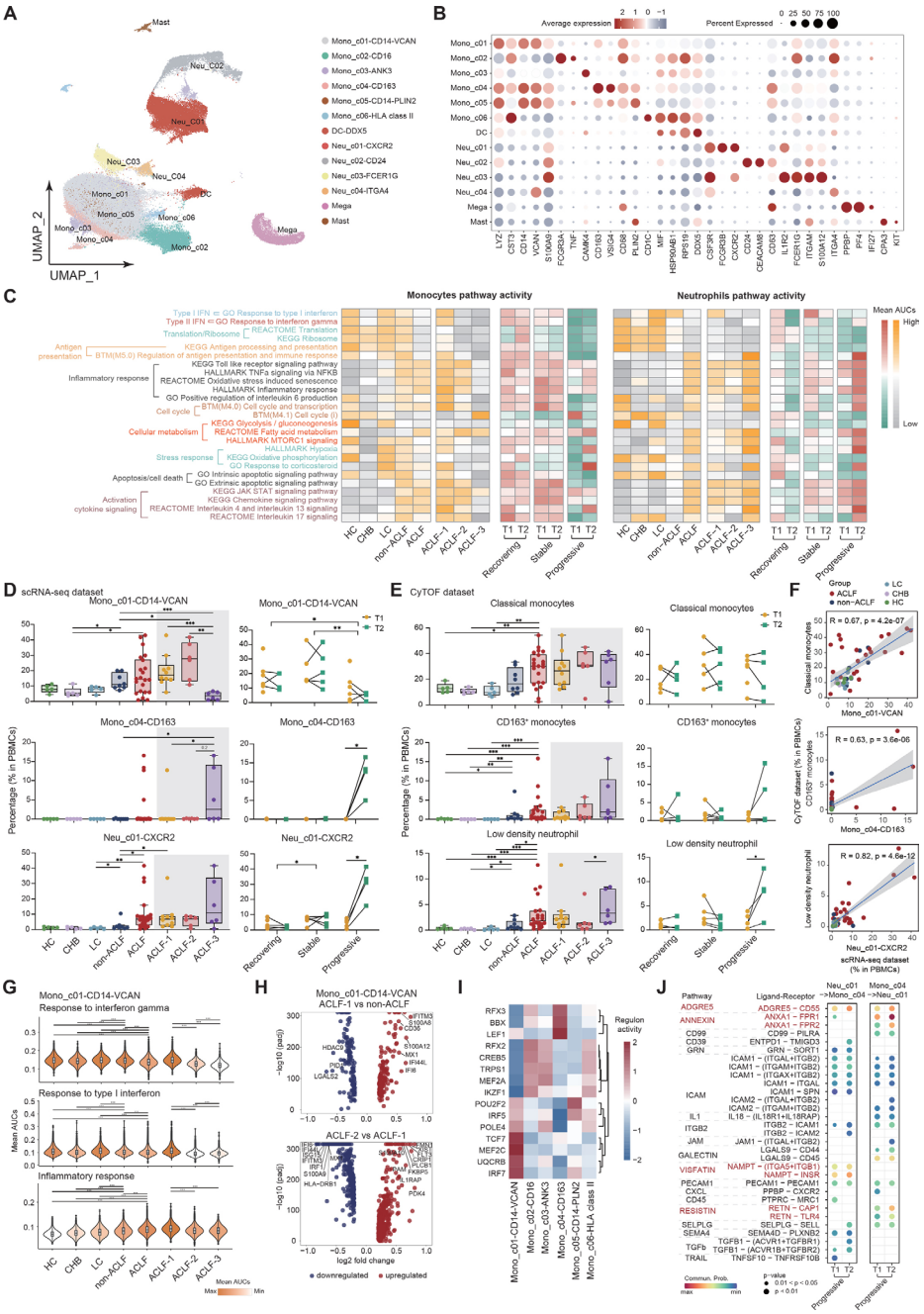

Figure 2 Disease-related longitudinal changes in myeloid cell subsets. (A) UMAP plot of myeloid cell subsets. (B) Dot plot for signature genes of myeloid cell subsets. Colours indicate increased (red) or decreased (blue) expression, and point size represents the number of cells per cluster expressing each gene. (C) Heatmap showing the scaled average functional scores of selected gene sets in monocytes (left) and neutrophils (right) across ACLF severity and progression. Gene sets were grouped into functional/pathway categories. (D, E) Plots showing proportions of Mono_c01-CD14-VCAN, Mono_c04-CD163 and Neu_c01-CXCR2 cells across ACLF severity (left: cross-sectional analysis, n=5/5/5/8/22/10/6/6, HC/CHB/LC/non-ACLF/ACLF/ACLF-1/ACLF-2/ACLF-3 groups, respectively) and across ACLF progression at two time points (right: longitudinal analysis) from (D) scRNA-seq and (E) CyTOF data. (F) Correlations of Mono_c01-CD14-VCAN, Mono_c04-CD163 and Neu_c01-CXCR2 proportions between scRNA-seq and CyTOF data. (G) Violin plots showing the functional signature scores of Mono_c01-CD14-VCAN subset across ACLF severity. (H) Volcano plot showing differentially expressed genes of Mono_c01-CD14-VCAN subset in ACLF-1 versus non-ACLF (upper) and in ACLF-2 versus ACLF-1 (lower). Thresholds: adjusted p value<0.01 and |log2-fold change|>0.2. (I) SCENIC analysis of TF activation enrichment in each monocyte subset. (J) Dot plot showing the interactions between Mono_c04-CD163 and Neu_c01-CXCR2 subsets in patients with progressive ACLF at two time points. Significant ligand–receptor pairs (p<0.05) are shown. Colour represents the communication probability. Signalling pathways with increasing probability at T2 are highlighted in red. *p value<0.05, **p value<0.01, ***p value<0.001 (Wilcoxon test or paired Wilcoxon test). ACLF, acute-on-chronic liver failure; AUC, area under the receiver operating characteristics curve; CHB, chronic hepatitis B; CyTOF, cytometry by time of flight; DC, dendritic cells; GO, gene ontology; HC, healthy control; IFN, interferon; KEGG, Kyoto encyclopedia of genes and genomes; LC, liver cirrhosis; NFKB, nuclear factor kappa B; PBMCs, peripheral blood mononuclear cells; scRNA-seq, single-cell RNA sequencing; TF, transcription factor; TNF, tumour necrosis factor; UMAP, uniform manifold approximation and projection; T1, sample collected at initial admission (within 24 hours); T2, sample collected the second time (within 2 weeks).

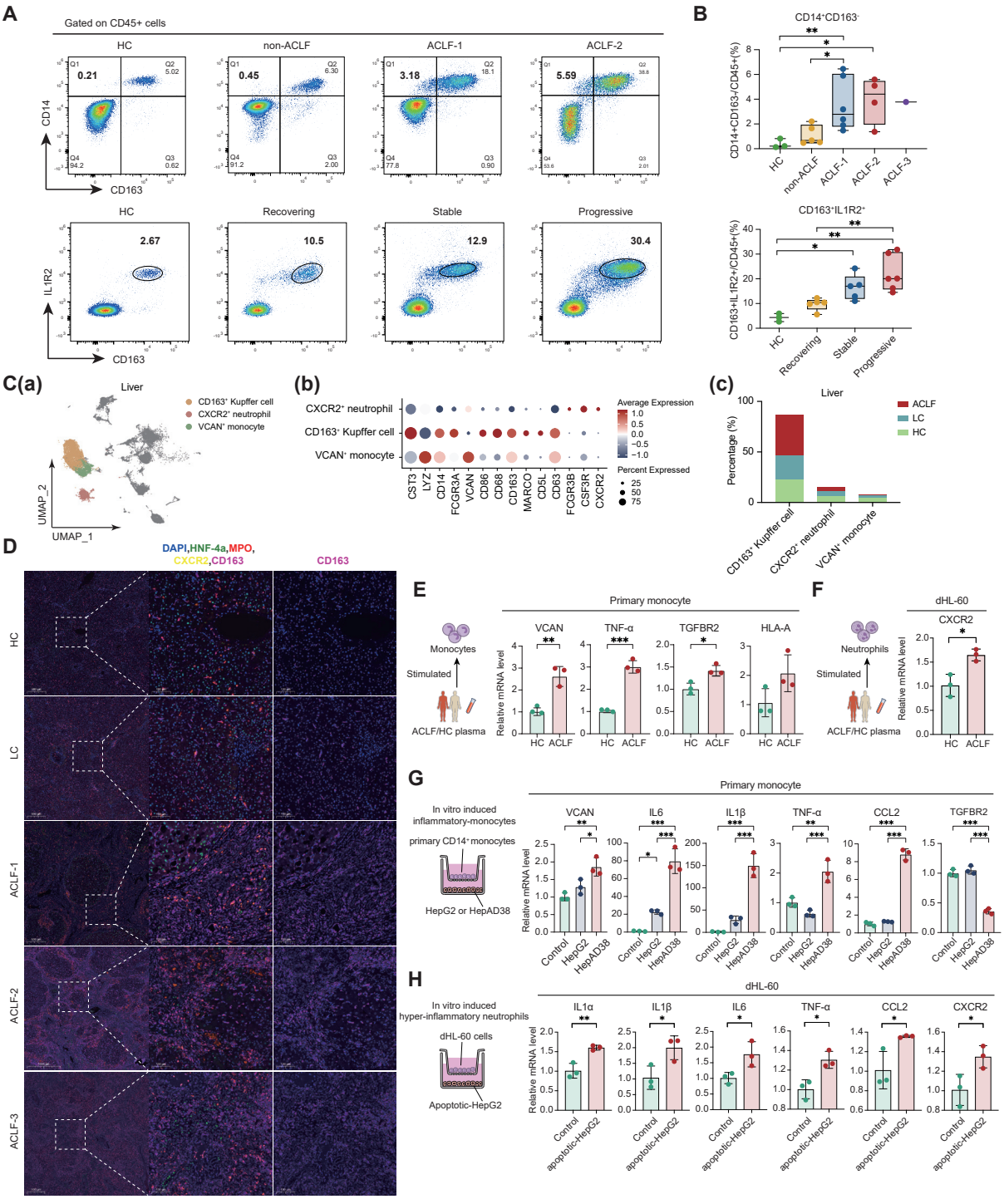

Figure 3 Characterisation of the hyperinflammatory microenvironment in HBV-ACLF progression. (A) Flow cytometric validation of $CD163^{+}IL1R2^{+}$ and $CD14^{+}CD163^{-}$ cells. Representative images showing the individual proportions of $CD163^{+}IL1R2^{+}$ and $CD14^{+}CD163^{-}$ cells at each stage across PBMC samples from patients and HCs. (B) Box plot showing proportions of $CD14^{+}CD163^{-}$ cells (upper, n=3/5/6/4/1, HC/non-ACLF/ACLF-1/ACLF-2/ACLF-3 groups) and $CD163^{+}IL1R2^{+}$ cells (lower, n=3/5/5/6, HC/recovering/stable/progressive groups) measured by flow cytometry. (C) (a–c) Enrichment of $CD163^{+}$ Kupffer cells, $CXCR2^{+}$ neutrophils and $VCAN^{+}$ monocytes in the ACLF liver tissues. (D) Multiplex immunofluorescence staining of hepatocytes (HNF-4a), $CXCR2^{+}$ neutrophils (MPO and CXCR2) and $CD163^{+}$ macrophages (CD163) in the liver tissue across HC, LC, ACLF-1, ACLF-2 and ACLF-3 groups. Representative images for each group are shown. (E) The expression levels of VCAN, TNF-α, TGFBR2 and HLA-A in primary monocytes on the stimulation of plasma from patients with ACLF or HC. (F) The expression levels of CXCR2 in neutrophil cell line dHL-60 on the stimulation of plasma from patients with ACLF or HC. (G) The expression levels of inflammatory-related genes in primary monocytes co-cultured with HepG2 and HepAD38 hepatocytes. (H) The expression levels of inflammatory cytokines in neutrophil cell line dHL-60 co-culture with or without apoptotic hepatocytes. *p value<0.05, **p value<0.01, ***p value<0.001 (unpaired t-test or ANOVA test). ACLF, acute-on-chronic liver failure; ANOVA, analysis of variance; HBV-ACLF, HBV-related ACLF; DAPI, 4′,6-diamidino-2-phenylindole; dHL-60, neutrophil-like differentiated HL-60 cells; HC, healthy control; HLA-A, human leukocyte antigen A; IL, interleukin; LC, liver cirrhosis; MPO, myeloperoxidase; PBMC, peripheral blood mononuclear cell; TGFBR2, transforming growth factor beta receptor 2; TNF, tumour necrotic factor; VCAN, versican.

of both cell types, suggesting a co-occurrence of hyperinflammation and anti-inflammation in the immune microenvironment of severe ACLF that contributed to disease deterioration (figure 3D).

Culturing primary monocytes with plasma from patients with ACLF or HC revealed that ACLF plasma stimulated higher expression of inflammatory-related genes (VCAN, TNF-α, TGFBR2, HLA-A) in monocytes than healthy plasma (figure 3E). Similarly, ACLF plasma induced significantly higher CXCR2 expression in neutrophil-like differentiated HL- 60 cells (figure 3F). Analysis of cytokine data revealed a significant increase in several cytokines, including growth differentiation factor 15 (GDF-15), secreted phosphoprotein 1 (SPP1) and interleukin (IL)-8 in the plasma of patients with ACLF (online supplemental figure 8). These results demonstrated that cytokines circulating in the blood of patients with ACLF could alter monocytes and neutrophils phenotypes. Co-culturing primary monocytes with the HBV-DNA-expressing human hepatocyte cell line HepAD38 or HepG2 cells showed that monocytes expressed significantly higher levels of proinflammatory genes (IL6, IL1β, versican (VCAN) and TNF-α) and chemotactic factor (C-C Motif Chemokine Ligand 2 (CCL2)) in the HepAD38 group (figure 3G). These results confirmed that HBV-DNA reactivation induced an inflammatory phenotype in monocytes during the early stage of ACLF. Considering the massive emergency of hyperinflammatory neutrophils in the end stage of ACLF, co-culturing dHL-60 cells with apoptotic HepG2 cells enhanced their inflammatory phenotype, marked by elevated expression of inflammatory-related genes (figure 3H).

These results suggest that an early inflammatory storm of $VCAN^+CD14^+$ monocytes triggered by HBV relapse is followed by apoptotic hepatocytes inducing hyper-inflammatory $CXCR2^+$ neutrophils and anti-inflammatory $CD163^+$ monocytes, creating a deleterious immune microenvironment and accelerating disease deterioration.

Restoration of cytotoxic T cells in patients recovering from ACLF

Given the dynamic T-cell changes during ACLF progression, we subclustered T cells into seven $CD8^+$, seven CD4+clusters and mucosal-associated invariant T (MAIT) cells in the scRNA-seq cohort (figure 4A). Gene signatures identified well-described T-cell clusters, including naïve (CD8T_c02-LEF1, CD8T_c07-SELL, CD4T_c02-CCR7), effector (CD8T_c01-GNLY, CD8T_c04-GZMA-PPBP and CD4T_c06-IGKC), effector memory (CD8T_c03-GZMK-COTL and CD4T_c01-ANXA1), recently activated effector memory or effector (CD8T_c05-TRDC), regulatory (CD4T_c04-FOXP3), central memory (CD4T_c03-BACH2), transient memory (CD4T_c05-PPBP) and exhausted (CD8T_c06-GZMK-GPR183, CD4T_c07-IFI44L) T cells (figure 4A–B, online supplemental figure 9A-D), (online supplemental Table 5). MAIT cells were characterised by high expression of SLC4A10.

The proportions of CD8T_c01-GNLY and CD8T_c03-GZMK-COTL1 decreased in ACLF but were gradually restored in recovering patients (figure 4C). CD8T_c01-GNLY had the highest cytotoxic score, while CD8T_c03-GZMK-COTL1 exhibited the highest inflammatory score (online supplemental figure 9C). Two effector $CD8^+$ T-cell clusters in the CyTOF data similarly normalised during disease recovery (figure 4D). The increased levels of migration marker CCR7 in ACLF indicated enhanced T-cell migration from blood to liver (online supplemental figure 10). Correlation analysis showed CD8T_c01-GNLY and CD8T_c03-GZMK-COTL1 were negatively associated with TB levels, INR and potassium levels and prognostic scores (online supplemental figure 9E). Functional restoration of these cells in recovering patients, particularly at T2, involved increased antigen presentation, inflammatory response and stress response (online supplemental figure 9G and I). Metabolic reduction in CD8T_c01-GNLY and CD8T_c03-GZMK-COTL1 observed in ACLF was reversed during recovery (online supplemental figure 9G-J). Alarmins S100A8 and S100A9 were significantly elevated in CD8T_c01-GNLY and CD8T_c03-GZMK-COTL1 of patients with ACLF (figure 4E). The functional changes of the two $CD8^+$ effector T-cell clusters were similar, with significantly differentially expressed genes (DEGs) between the ACLF and non-ACLF groups mainly involved in defence response, type II interferon response, viral process and antigen processing and presentation (figure 4F–G). $CD8^+$ naïve T cells (CD8T_c02-LEF1) were depleted in patients with severe ACLF and negatively correlated with age (online supplemental figure 9F).

MAIT cells, innate-like lymphocytic cells, declined in ACLF, with significantly lower proportions in progressive than recovering patients (figure 4C). MAIT cells had high cytotoxic and inflammatory scores (online supplemental figure 9D). The CyTOF data confirmed consistent alterations in MAIT cell proportions across ACLF severity (figure 4D). Reactivation in recovering patients involved hypoxia and oxidative phosphorylation, similar to cytotoxic $CD8^+$ T cell reactivation (figure 4H). These results indicate that the cytotoxic T-cell response may regulate HBV replication in HBV-ACLF and facilitate disease recovery.

$CXCR2^+$ neutrophils inhibit cytotoxic T cells

We further investigated the mechanisms underlying cytotoxic T-cell exhaustion in the patients with severe ACLF. Correlation analysis showed a significant negative association between proportions of CD8T_c01-GNLY, CD8T_c03-GZMK-COTL1 and MAIT with Neu_c01-CXCR2, consistent with CyTOF results (figure 5A–B). Immunosuppression-related genes, such as arginase 1 (ARG1), cystatin F and membrane metalloendopetidase, were highly expressed in Neu_c01-CXCR2 of patients with ACLF (figure 5C). scRNA-seq analysis of liver tissues from HC, patients with LC and ACLF identified $CD8^+$ effector T cells and MAIT cells, which were decreased in ACLF livers and negatively correlated with $CXCR2^+$ neutrophils (figure 5D). These results indicate that Neu_c01-CXCR2 exerts the immunosuppressive effects, promoting the exhaustion of cytotoxic T-cells.

Multiplex immunofluorescence staining assessed spatial relationships between MAIT cells, cytotoxic $CD8^+$ T cells and $CXCR2^+$ neutrophils in liver tissues from HC and patients with LC and ACLF (figure 5E). MAIT cells and cytotoxic $CD8^+$ T cells increased in ACLF-1, suggesting their migration from circulating blood to the liver to target HBV-relapsed hepatocytes. $CXCR2^+$ neutrophils were highly enriched in the liver of patients with ACLF-3 and were found in close proximity to cytotoxic $CD8^+$ T cells, whose proportion declined. Correlation analysis revealed a negative association between the proportion of $CXCR2^+$ neutrophils and those of cytotoxic $CD8^+$ T cells and MAIT cells in patients with ACLF. To further verify the potential immunosuppressive effect of $CXCR2^+$ neutrophils on T cells, we performed co-culture of $CXCR2^+$ and $CXCR2^-$ neutrophils from dHL-60 cells with blood-derived $CD3^+$ T cells (stimulated with anti-CD3/CD28) (figure 5F,H). Compared with $CXCR2^-$ neutrophils, co-culture with $CXCR2^+$ neutrophils markedly decreased the percentage of granzyme B $(GZMB)^+CD8^+$ T cells and increased the fraction of exhausted $CD8^+PD1^+$ T cells,

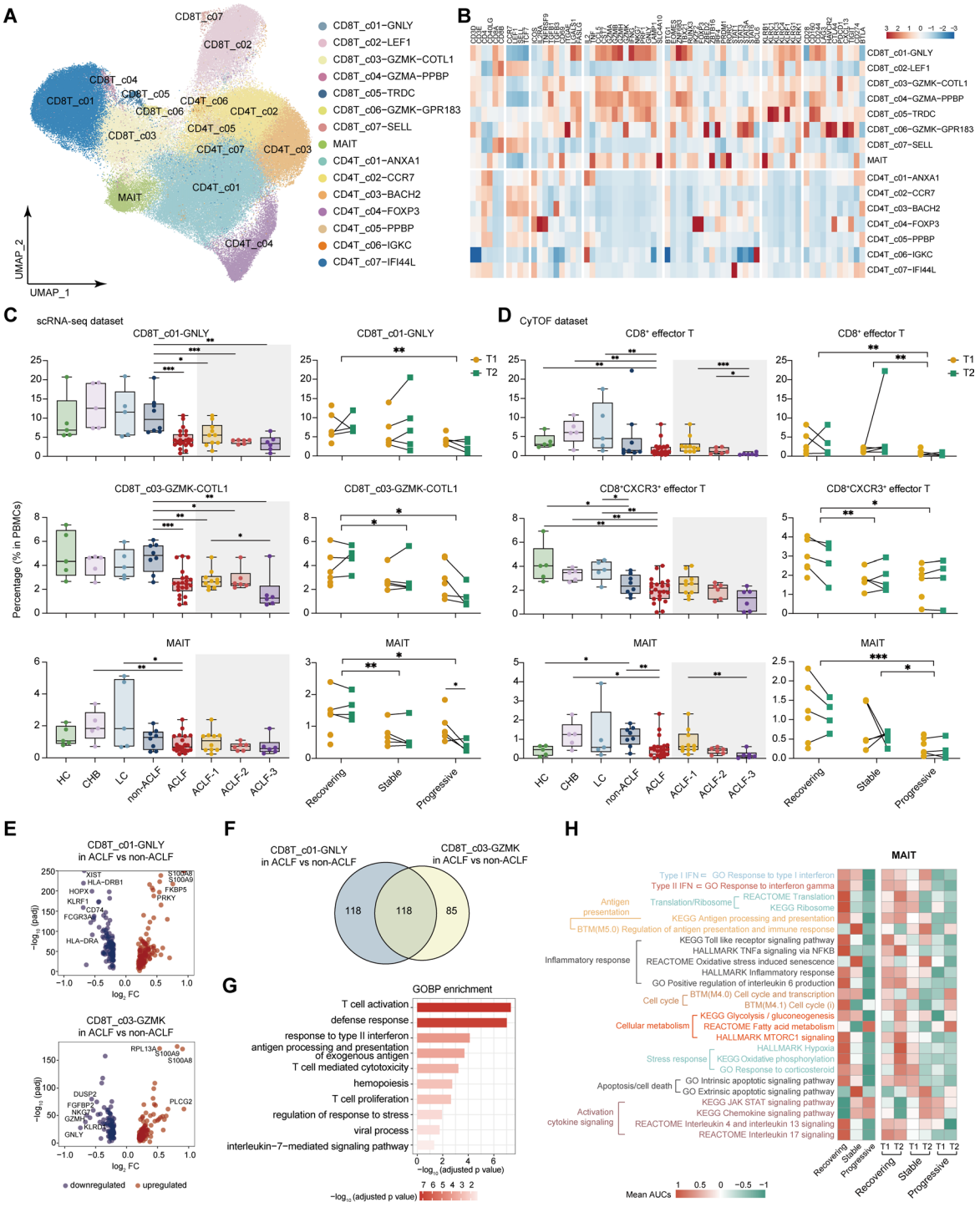

Figure 4 Impaired cytotoxic T-cell response during ACLF progression. (A) UMAP plots of T-cell subsets. (B) Heatmap of functional markers used to annotate T-cell subsets. (C, D) Plots showing proportions of CD8T_c01-GNLY, CD8T_c03-GZMK-COTL1 and MAIT cells across ACLF severity (left: cross-sectional analysis, n=5/5/5/8/22/10/6/6, HC/CHB/LC/non-ACLF/ACLF/ACLF-1/ACLF-2/ACLF-3 groups, respectively) and across ACLF progression at two time points (right: longitudinal analysis) from (C) scRNA-seq and (D) CyTOF data. (E) Volcano plots showing DEGs in CD8T_c01-GNLY (upper) and CD8T_c03-GZMK (lower) subsets (ACLF vs non-ACLF). Thresholds: adjusted p value<0.01 and |log2-fold change|>0.2. (F) Venn diagram showing the shared DEGs between CD8T_c01-GNLY and CD8T_c03-GZMK in ACLF versus non-ACLF. (G) Functional enrichment analysis of 118 overlapping DEGs between CD8T_c01-GNLY and CD8T_c03-GZMK in patients with ACLF versus without ACLF, showing the top 10 significant terms ranked by adjusted p values. (H) Heatmap showing the scaled average functional scores of selected gene sets in the MAIT subset during ACLF progression. Gene sets were grouped into functional/pathway categories. ACLF, acute-on-chronic liver failure; AUC, area under the receiver operating characteristics curve; CHB, chronic hepatitis B; CyTOF, cytometry by time of flight; DEGs, differentially expressed genes; GOBP, gene ontology biological process; GO, gene ontology; HC, healthy control; IFN, interferon; KEGG, Kyoto encyclopedia of genes and genomes; LC, liver cirrhosis; MAIT, mucosal-associated invariant T; NFKB, nuclear factor kappa B; PBMCs, peripheral blood mononuclear cells; scRNA-seq, single-cell RNA sequencing; TNF, tumour necrosis factor; UMAP, uniform manifold approximation and projection; T1, sample collected at initial admission (within 24 hours); T2, sample collected the second time (within 2 weeks).

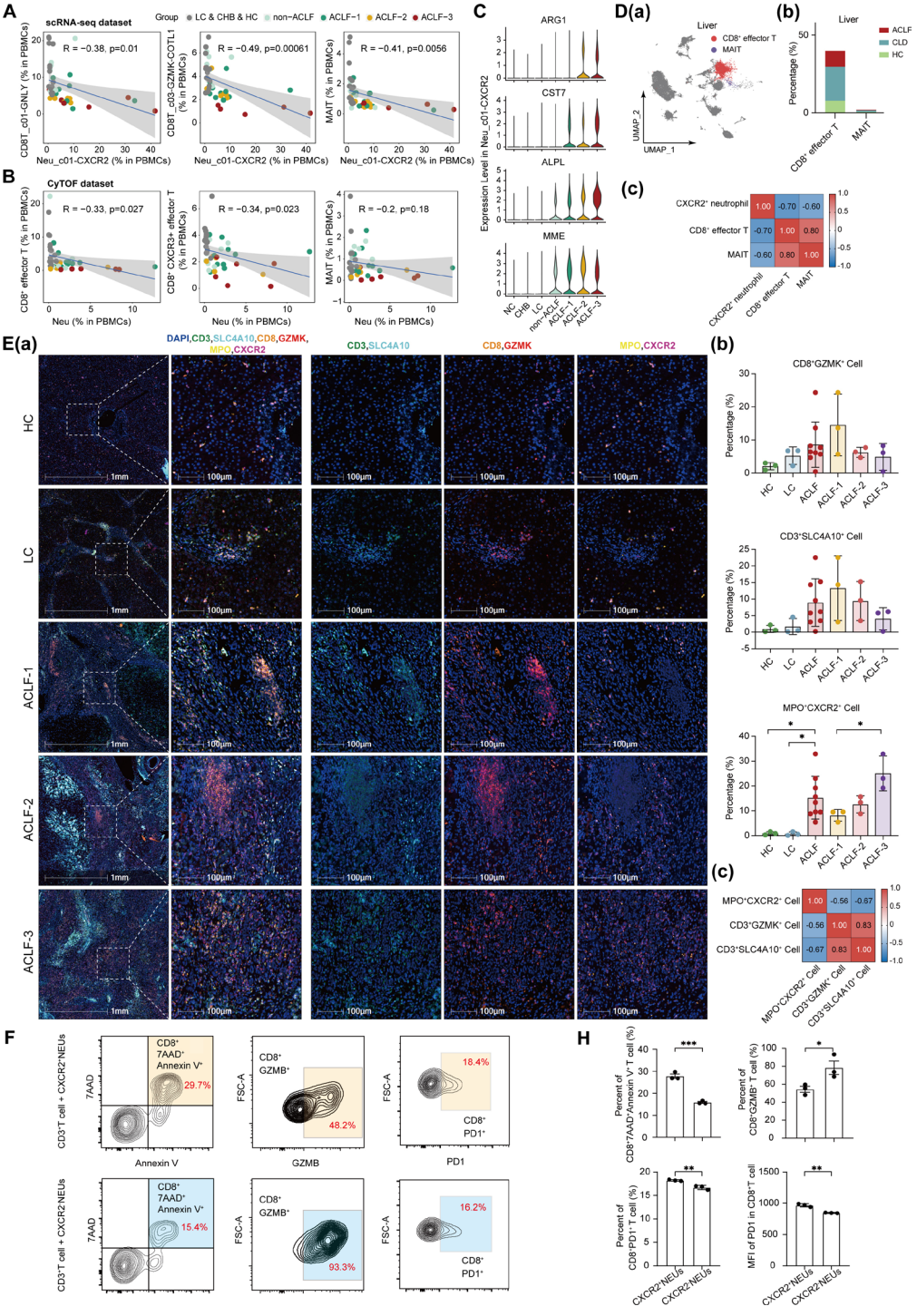

Figure 5 Hyperinflammatory neutrophils drive cytotoxic T-cell exhaustion. (A, B) Correlations of Neu_c01-CXCR2 proportions with CD8T_c01-GNLY, CD8T_c03-GZMK-COTL1 and MAIT from scRNA-seq (A) and CyTOF (B) data. (C) Immunosuppressive gene expression in Neu_c01-CXCR2 across ACLF severity. (D) (a–c) Enrichment of $CD8^+$ effector T and MAIT cells in the ACLF liver tissues. (E) (a–c) Multiplex immunofluorescence staining of effector $CD8^+$ T cells (CD8 and GZMK), MAIT (CD3 and SLC4A10) and $CXCR2^+$ neutrophils (MPO and CXCR2) in the liver tissues across HC, LC, ACLF-1, ACLF-2 and ACLF-3 groups. Representative images for each group are shown (a). Bar plot showing the quantified results of each double-positive cell in the groups (b). Correlations of $CXCR2^+$ neutrophil proportions with effector $CD8^+$ T and MAIT cells in ACLF (c). (F) Representative flow cytometry images showing the proportions of $CD8^+GZMB^+$ T cells, $CD8^+$ $7AAD^+Annexin\ V^+$ T and $CD8^+PD1^+$ cells in $CXCR2^+$ or $CXCR2^-$ neutrophils co-cultured with $CD45^+CD3^+$ T cells from blood of HCs activated with anti-CD3/CD28 antibodies. (H) Bar plot showing the quantified results of $CD8^+GZMB^+$ T cells, $CD8^+7AAD^+Annexin\ V^+$ T cells, $CD8^+PD1^+$ T cells and mean fluorescence intensity (MFI) of PD1 in $CD8^+$ T cells. *p value<0.05, **p value<0.01, ***p value<0.001 (unpaired t test or ANOVA test). ACLF, acute-on-chronic liver failure; ALPL, Alkaline Phosphatase, Biomineralization Associated; ANOVA, analysis of variance; ARG1, arginase 1; CHB, chronic hepatitis B; CST7, cystatin F; CXCR2, C-X-C motif chemokine receptor 2; CyTOF, cytometry by time of flight; DAPI, 4′,6-diamidino-2-phenylindole; HC, healthy control; FSC-A, forward scatter area; GZMK, granzyme K; LC, liver cirrhosis; MAIT, mucosal-associated invariant T; MME, membrane metalloendopetidase; MPO, myeloperoxidase; PBMCs, peripheral blood mononuclear cells; PD1, programmed cell death protein 1; scRNA-seq, single-cell RNA sequencing; SLC4A10, solute carrier family 4 member 10; 7AAD, 7-amino-actinomycin D.

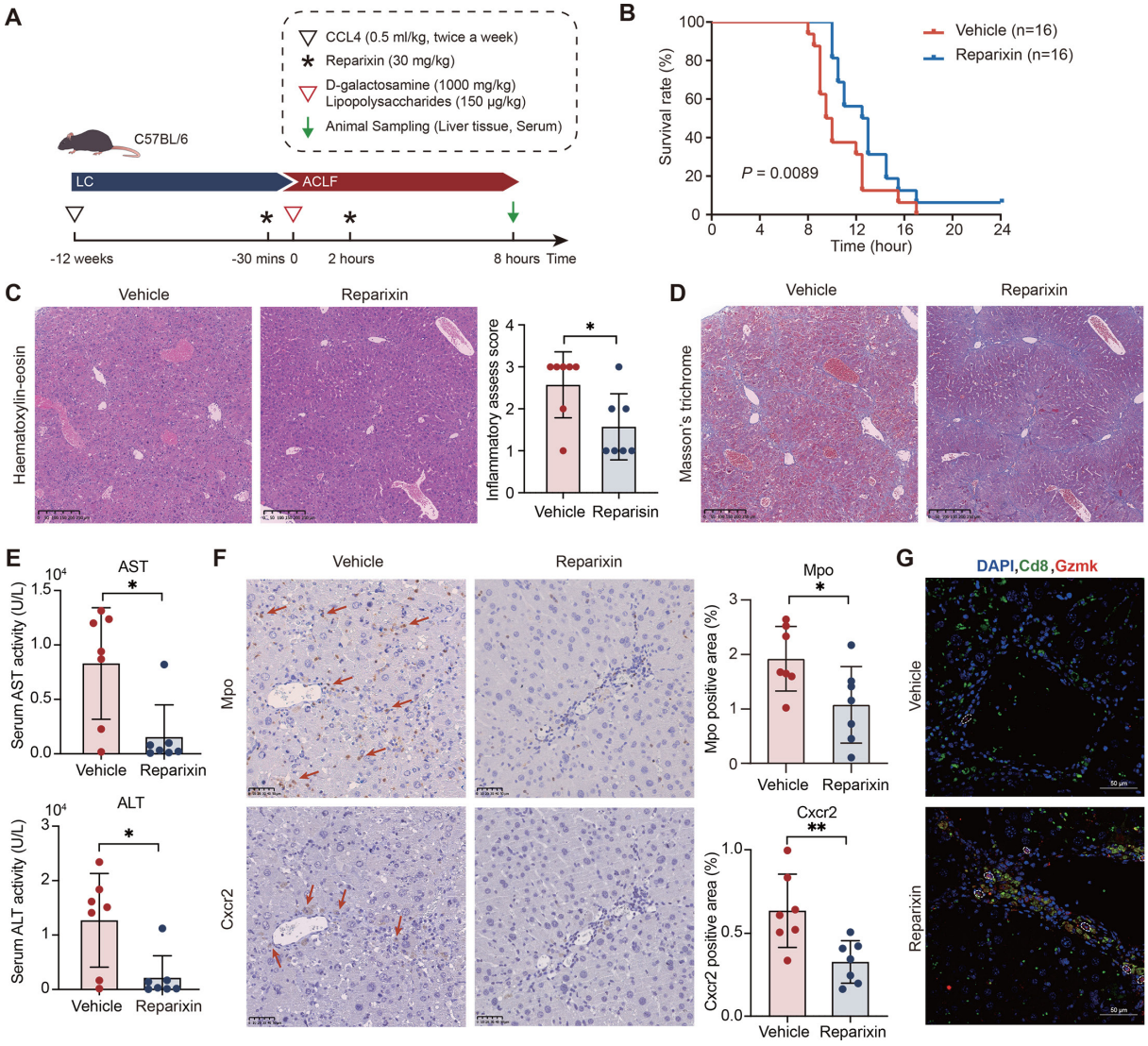

Figure 6 Effects of CXCR2 inhibitor reparixin treatment in ACLF mouse models. (A) Schematic design for the administration of CXCR2 inhibitor reparixin in ACLF mouse models. (B) Survival analysis of ACLF mice treated with or without reparixin. (C) H&E staining of liver tissues from two groups (left). Inflammatory score of H&E staining in the two groups (right). (D) Masson's trichrome staining of liver tissues from two groups. (E) Changes in two typical biochemical markers of liver function observed in the two groups. (F) Immunohistochemical staining for Mpo and Cxcr2 in liver tissues from two groups. (G) Multiplex immunofluorescence staining of cytotoxic $CD8^+$ T cells (Cd8 and Gzmk) in liver tissues from two groups. *p value<0.05, **p value<0.01 (unpaired t test), n=7/group. ACLF, acute-on-chronic liver failure; ALT, alanine aminotransferase; AST, aspartate aminotransferase; CCL, C-C motif chemokine ligand; Cxcr2, C-x-c motif chemokine receptor 2; DAPI, 4′,6-diamidino-2-phenylindole; Gzmk, granzyme k; LC, liver cirrhosis.

confirming $CXCR2^+$ neutrophils could suppress $CD8^+$ T cells cytotoxicity. Immunohistochemistry staining showed significantly high programmed cell death protein 1 (PD1) expression in liver tissue (online supplemental figure 11).

Taken together, these results indicate that the significant enrichment of $CXCR2^+$ neutrophils in severe ACLF contributes to the suppression of cytotoxic T cells, thereby accelerating the deterioration of ACLF.

CXCR2 inhibitor rescues ACLF mice

Given the critical role of $CXCR2^+$ neutrophils in the pathogenesis of ACLF, we hypothesised that CXCR2 inhibition could alleviate liver failure via regulating neutrophils and restoring cytotoxic T cells. To assess the therapeutic effect of CXCR2 inhibition, we administered reparixin, a CXCR2 inhibitor, to an ACLF mouse model induced by injecting D-galactosamine and lipopolysaccharides in CCL4-treated mice (figure 6A). Survival analysis showed that reparixin treatment notably improved the survival of ACLF mice (figure 6B). H&E and Masson's trichrome staining demonstrated histological improvement after reparixin treatment, including reduced hepatocellular necrosis, fewer haemorrhage and less inflammatory cell infiltration (figure 6C,D). Biochemical analysis revealed significantly decreased levels of serum alanine aminotransferase (ALT) and aspartate aminotransferase (AST) in the reparixin treatment group (figure 6E). Immunohistochemistry staining confirmed significantly lower Mpo and Cxcr2 expression, indicating the less infiltration of neutrophils after reparixin treatment (figure 6F). Multiplex immunofluorescence staining showed the increased cytotoxic $CD8^+$ T cells (figure 6G). These results demonstrated the therapeutic effect of the CXCR2 inhibitor reparixin in ACLF and its potential to improve survival.

Generalisability and specificity of the immune cell dynamics in ACLF

To further assess the robustness of our findings, we included patients with out HBV-ACLF to evaluate their generalisability across different aetiologies, and sepsis patients without liver disease to examine the liver-specificity of the observed immune alterations. scRNA-seq analysis showed no significant differences in the proportions of the targeted immune clusters between patients with HBV-ACLF and non-HBV-ACLF, except for Mono_c04-CD163, which was more abundant in non-HBV-ACLF (figure 7A). Sepsis patients exhibited a higher proportion of Mono_c04-CD163 and a lower proportion of Neu_c01-CXCR2. CD8T_c01-GNLY and MAIT were decreased in both patients with ACLF and sepsis. These findings were further validated using bulk RNA-seq data from larger cohorts through CIBERSORTx deconvolution analysis (figure 7B). We observed notable differences in myeloid cell profiles between ACLF and sepsis, characterised by increased Mono_c04-CD163 and decreased Mono_c01-CD14-VCAN and Neu_c01-CXCR2 in sepsis. Functional analysis showed that pathway activities within the targeted immune clusters were largely consistent between patients with HBV-ACLF and non-HBV-ACLF but remained unchanged in the sepsis, underscoring the liver-specific nature of these immune responses (figure 7C).

Considering the lack of consensus on ACLF classification, we reclassified patients based on European Association for the Study of Liver-Chronic Liver Failure (EASL-CLIF) criteria and reanalysed the cellular trajectories. The results revealed similar patterns, with $CD163^+$ monocytes and $CXCR2^+$ neutrophils increasing at the end stage of ACLF, while $CD8^+$ effector T cells were gradually restored in recovering patients (online supplemental figure 12).

Cellular module analysis reveals six immune patterns in ACLF

We analysed co-enrichment patterns of immune cells in 30 PBMC samples from 17 patients to investigate the peripheral immune microenvironment subtypes during ACLF progression. Hierarchy clustering analysis identified six cellular modules (CM1–CM6), stratifying samples into six distinct immune pattern subtypes (figure 7D,E, (online supplemental Table 6). Properties of each cellular module, including cell cluster, cytokine expression, cellular interactions and functional signatures, were investigated (online supplemental figure 13). CM1 contained naïve T cells with high LTB expression and low interferon (IFN) response, inflammatory response and hypoxia, indicating an initial immune activation state. CM2, contained effector T and NK cells, exhibiting the highest antigen processing and presentation, as well as an effective inflammatory response. Samples enriched with CM2 were from recovering patients, suggesting that CM2 is associated with favourable outcomes. CM3, comprising classical and non-classical monocytes, was found in patients with mild ACLF (ACLF-1/2) with variable outcomes, indicating treatment-dependent disease trajectories. CM4, a mix-cell module, was linked to favourable outcomes. CM5, associated with 28-day mortality, showed enriched thrombospondin (THBS) signalling, with decreased IFN response and antigen presentation contributing to poor outcomes. CM6 contained myeloid cells (Mono_c04-CD163, Neu_c01-CXCR2, Neu_c02-CD24 and Neu_c03-FCER1G) with high inflammatory response, TNFa signalling via NFKB and hypoxia, exacerbating the systemic inflammation in the end stage of ACLF and worse prognosis. Anti-inflammatory interactions (ENTPD1-TMIGD3, ANXA1-FPR2 and IL1B-IL1R2 ligand–receptor pairs) in CM6 suggested a compensatory response to hyperinflammation.

Risk stratification using CM2 and CM6 signatures from bulk RNA-seq data of HBV-ACLF and non-HBV-ACLF samples revealed significant differences in the cumulative incidence of progressive ACLF (figure 7F). Specifically, high CM6 signature and low CM2 signature expression were associated with worse outcomes in ACLF, regardless of aetiology. These results validate the robustness of the immune pattern classification and its potential clinical application.

DISCUSSION

Dysregulation of immune responses has been implicated in ACLF development.[4 7] Longitudinal studies are urgently needed to clarify the dynamic changes in the cellular and molecular processes driving the progression from chronic liver disease to ACLF. In this study, we jointly conducted single-cell transcriptomics and proteomics to construct a single-cell atlas of circulating immune cells in HBV-ACLF, providing a detailed view of the dynamic immune response over time. Our multimodal approach, which incorporates analysis at both the RNA and protein levels, greatly increases the robustness and reliability of the results. The clinical relevance of results was confirmed through bulk transcriptome analysis of numerous samples from both prospective COSSH-ACLF and non-HBV-ACLF cohorts.

The innate immune response, a first line of defence, plays a major role in ACLF pathophysiology. The CANONIC study indicated that a dysregulated innate immune response might be the predominant mechanism of ALD-ACLF.[4] Increased proportions of monocytes and neutrophils detected by flow cytometry have been reported to correlate with ACLF severity.[15–17] Our previous studies based on bulk transcriptomics showed innate immune dysfunction in patients with ACLF, with upregulated monocyte-related, neutrophil-related and inflammation-related gene signatures.[7 18] However, the dynamics of immune cell changes during ACLF progression and their impact on patient outcomes remain unelucidated. This study observed significant myeloid cell changes over time in ACLF, particularly in progressive patients. Elevated IFN response in $VCAN^+CD14^+$ monocytes in the early stage of ACLF indicates a rapid response to viral relapse, suggesting that HBV reactivation triggers ACLF and leads to proinflammatory responses. High cytokine and inflammatory scores in $VCAN^+CD14^+$ monocytes imply that these cells might be a major source of early ACLF inflammatory storms.[19] Low-density mature neutrophils with hyperinflammation were prominent in patients with progressive ACLF, likely triggered by secondary bacterial infections due to their role as 'first responders' against invading microbes and bacteria.[20 21] The damage-associated molecular patterns released by injured hepatocytes further contributed to neutrophils dysfunction.[22] The activation of neutrophils triggers degranulation and a decrease in their buoyant density due to alterations in granule content and nuclear morphology, causing them to settle with the PBMCs as LDNs.[23] Their reduced homing capacity and escape from macrophage efferocytosis may contribute to subsequent tissue damage.[20 21 24] $CD163^+$ monocytes with anti-inflammatory phenotypes in the end stage of ACLF suggest immune paralysis and worsened outcomes. Studies have reported that patients with ACLF show increased immunosuppressive macrophages in the liver, leading to a high percentage of reverse migrated monocytes/macrophages with a $CD163^{high}$ phenotype in circulation, contributing to increased susceptibility to infections and greater

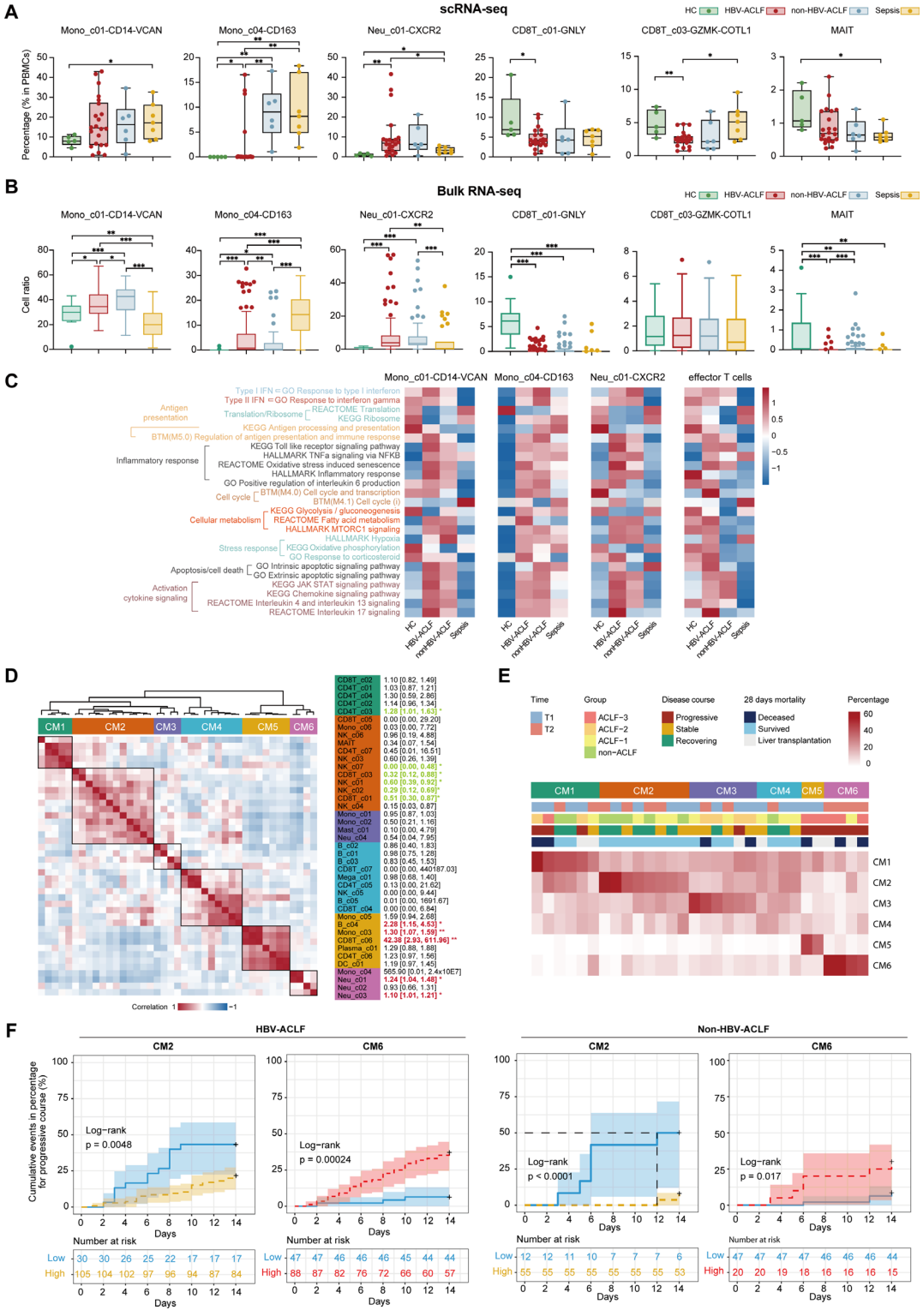

Figure 7 Identified six cellular modules associated with ACLF progression (A) The proportions of targeted immune cell subsets among HC, patients with HBV-ACLF, patients with non-HBV-ACLF and patients with sepsis based on scRNA-seq data. (B) The relative changes in the abundance of targeted immune cell subsets estimated by CIBERSORTx cellular composition analysis of bulk RNA-seq data. (C) Heatmap showing the scaled average functional scores of selected gene sets within targeted immune cell subsets across HC, HBV-ACLF, non-HBV-ACLF and sepsis. (D) Six cellular modules identified based on the correlations of cell clusters from patients with HBV-ACLF and patients with early stage non-ACLF. HR of each cell cluster based on 28-day mortality shown on the right (Cox regression). (E) Percentage of CM1-CM6 among patients with HBV-ACLF and patients with early stage non-ACLF. (F) Cumulative event analysis of patients stratified by CM2 and CM6 gene signatures using bulk RNA-seq data from patients with HBV-ACLF (left) and patients with non-HBV-ACLF (right). Log-rank test. ACLF, acute-on-chronic liver failure; CM, cellular module; GO, gene ontology; HBV-ACLF, HBV-related ACLF; HC, healthy control; IFN, interferon; KEGG, Kyoto encyclopedia of genes and genomes; MAIT, mucosal-associated invariant T; NFKB, nuclear factor kappa B; PBMCs, peripheral blood mononuclear cells; scRNA-seq, single-cell RNA sequencing; TNF, tumour necrosis factor; T1, sample collected at initial admission (within 24 hours); T2, sample collected the second time (within 2 weeks).

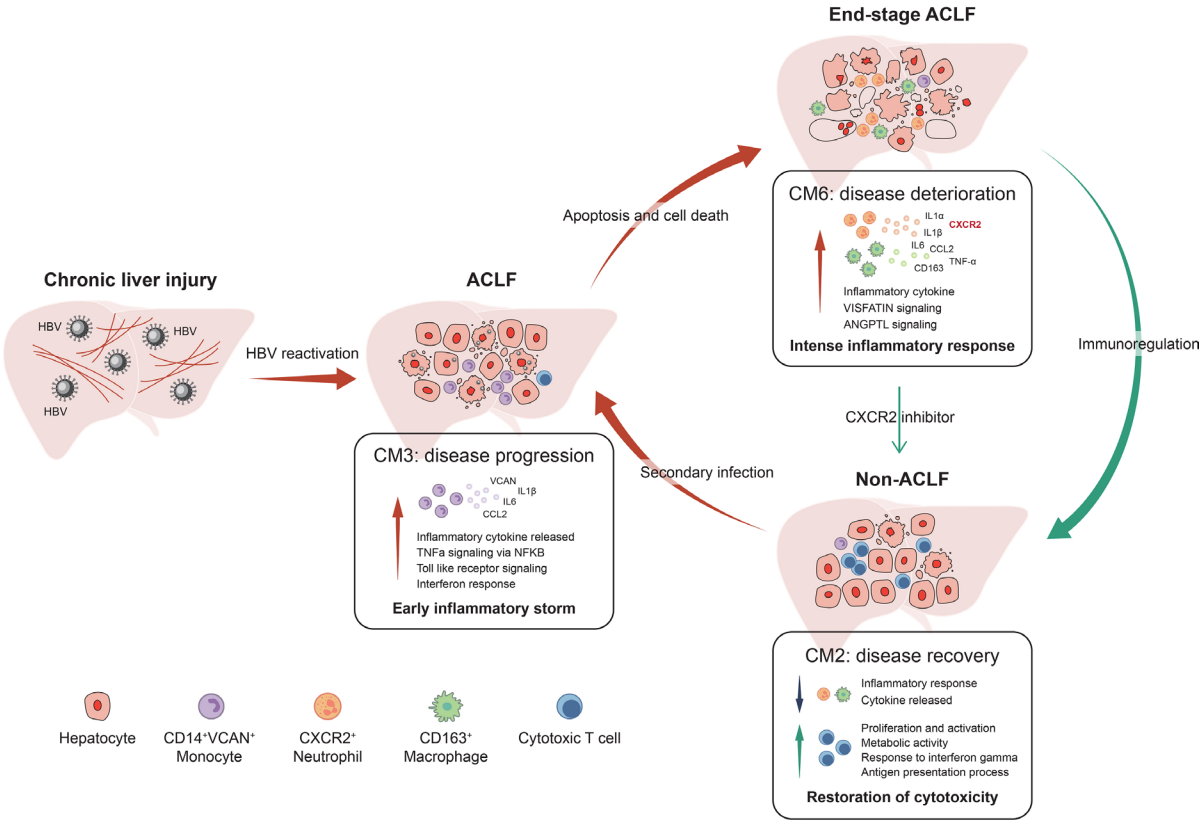

Figure 8 Graphical schematic of HBV-ACLF development and progression. HBV-ACLF is initiated by HBV relapse, with increased classical monocytes and inflammatory signalling in early stage (CM3 immune pattern). This disease stage could be considered an early optimal therapeutic window. Hyperinflammatory neutrophils and CD163$^+$ monocytes with anti-inflammatory phenotype are associated with the end stage of HBV-ACLF (CM6 immune pattern). A robust adaptive immune response, with increased cytotoxic T cells and enhanced antigen presentation, marks disease recovery (CM2 immune pattern). ACLF, acute-on-chronic liver failure; CCL, C-C motif chemokine ligand; CM, cellular module; CXCR, C-X-C motif chemokine receptor; HBV-ACLF, HBV-related ACLF; IL, interleukin; NFKB, nuclear factor kappa B; TNF, tumour necrosis factor; VCAN, versican.

disease severity.[16 25] Overall, the innate immune response plays distinct roles in different stages of ACLF.

The mechanism of T cell exhaustion in ACLF remains unclear.[17 18] This study found T cell exhaustion in ACLF, characterised by reduced numbers, cytotoxic function and metabolic activity. Studies showed that exhausted T cells expand in HBV-ACLF, with B and T lymphocyte associated (BTLA)-mediated CD4+T cell exhaustion increasing infection and mortality risk.[26 27] Activated neutrophils promote T-cell exhaustion, impairing the adaptive immune response and inducing excessive innate responses.[28 29] T-cell response in ACLF is limited by the decreasing proportion of naïve T cells with age, leading to poor outcomes in elderly patients.[1 30 31] Effector CD8$^+$ T cells play a role in liver immune surveillance, impaired by persistent liver damage.[32] Studies have reported that higher frequencies of functional T cell responses provide insights into immunotherapeutic approaches for HBV infection and its complications.[33 34] Restoration of effector T cells in recovering patients suggests that addressing lymphopenia might be a potential treatment to improve clinical outcomes in patients with ACLF. Analysing adaptive immune cells in peripheral blood appears to be a reliable strategy to track disease improvement.

Immune dysfunction plays a critical role in ACLF, highlighting the potential of immune-based therapies. However, effective therapies to counteract immune dysfunction in ACLF remain lacking. MerTK$^+$ monocytes and tissue macrophages emerge in ACLF, with the MerTK inhibitor UNC*569* restoring proinflammatory cytokines and potentially alleviating immune paralysis.[16] Granulocyte-colony stimulating factor may reduce neutrophil fever by inducing endogenous neutrophils and has been reported to improve survival of ACLF; however, its use remains controversial.[35 36] Future therapeutic strategies require a deeper understanding of immune-regulating cellular networks and signalling pathways, as well as identifying the key molecular triggers underlying immune dysfunction.[37] Our longitudinal single-cell multiomics analysis identified CXCR2$^+$ neutrophils as central to ACLF pathogenesis. These neutrophils induced hyperinflammation alongside anti-inflammatory CD163$^+$ macrophages and suppressed cytotoxic CD8$^+$ T cells, contributing to the deterioration of the immune microenvironment. CXCR2$^+$ neutrophils have been shown to be prevalent in hepatocellular carcinoma where they promote tumour progression, and combination immunotherapy with a CXCR2 antagonist can modulate neutrophils phenotype and enhance the efficacy of anti-PD1 therapy.[38] In cholestatic liver injury, CXCR2 facilitates neutrophil recruitment, contributing to liver damage.[39] Evidence has shown that CXCR2$^+$ polymorphonuclear myeloid-derived suppressor cells, a subset of immunosuppressive neutrophils, accumulate in the liver and contribute to the progression of cholangiocarcinoma.[40 41] Although systemic CXCR2 inhibition may affect multiple cell types, the significantly elevated IL-8—the primary CXCR2 ligand responsible for neutrophil chemotaxis—in patients with ACLF suggests that neutrophil recruitment is a key targetable pathway. Our validations demonstrated that selective targeting of neutrophils with the CXCR2 inhibitor raparixin significantly reduced ACLF mouse mortality by decreasing

neutrophils infiltration and enhancing cytotoxic $CD8^+$ T cells activation.

Our results illustrate a potential collaborative crosstalk between the innate and adaptive immune systems during ACLF progression, where HBV relapse may induce $VCAN^+CD14^+$ monocytes to adopt pro-inflammatory phenotype and trigger ACLF, followed by apoptotic hepatocytes promoting the accumulation of highly inflammatory $CXCR2^+$ neutrophils and the exhaustion of cytotoxic T cells, ultimately contributing to ACLF deterioration (figure 8). Six cellular modules identified through unbiased stratification of immune responses in ACLF could serve as a tool to reflect disease states and guide immunotherapies. The CM3-dominant stage, characterised by early inflammatory pathologies, could be an optimal therapeutic window. Therapies such as hormone treatments to suppress inflammation in this stage may prevent disease progression.[42 43] The CM6 subtype, associated with systemic inflammation and deteriorating ACLF, suggests that targeted immunotherapy, such as CXCR2 inhibition, could effectively alter prognosis. And liver transplantation for patients in this immune subtype may offer survival benefit. The CM2 subtype with high activated lymphocyte frequency suggests the effectiveness of treatment and indicates signs of recovery. This stratification framework provides detailed insights into ACLF pathophysiology and raises the prospect of developing more personalised intervention strategies.

This study has several limitations. The relatively small sample size of our cohort does not allow us to thoroughly evaluate the contributions of aetiology, precipitating events and organ failure across the course of disease progression. Further validation with more patients in larger and diverse cohorts, including non-liver disease controls, is helpful to enhance our understanding of ACLF pathogenesis. Although our study provides important insights into circulating immune cell dynamics, the proposed immune cell crosstalk, inferred from integrated experimental and transcriptomic analyses, requires further investigation and validation—particularly through intrahepatic immune profiling from large samples and gene-specific knock-in/knock-out models. T-cell receptor and B-cell receptor sequencing, along with antigen-specific cell labelling, are needed in future studies to distinguish HBV-specific from non-specific immune activation in HBV-ACLF.

In summary, our longitudinal multimodal assessment of circulating immune cells at single-cell resolution comprehensively revealed dynamic immune response changes during HBV-ACLF. Stratified immune patterns present new directions for precision immunotherapy. Our multiomics single-cell data from longitudinal study offer valuable insights into the peripheral immune system in ACLF. These findings provide mechanistic insights into immune cell roles in ACLF progression and potential biomarkers for disease monitoring.

Author affiliations
[1]State Key Laboratory for Diagnosis and Treatment of Infectious Diseases, National Clinical Research Center for Infectious Diseases, National Medical Center for Infectious Diseases, Collaborative Innovation Center for Diagnosis and Treatment of Infectious Diseases, The First Affiliated Hospital, Zhejiang University School of Medicine, Hangzhou, Zhejiang, China
[2]Department of Gastroenterology, Zhejiang Provincial People's Hospital, People's Hospital Affiliated of Hangzhou Medical College, Hangzhou, China
[3]Transplantation Center, The Third Xiangya Hospital, Central South University, Changsha, China
[4]NHC Key Laboratory of Translational Research on Transplantation Medicine, Changsha, China
[5]Department of Gastroenterology, The First Affiliated Hospital, Zhejiang University School of Medicine, Hangzhou, Zhejiang, China
[6]Institute of Big Data and Artificial Intelligence in Medicine, School of Electronics and Information Engineering, Taizhou University, Taizhou, Zhejiang, China
[7]BioRigino Co Ltd, Anji, China
[8]Department of Severe Hepatology, Hangzhou Xixi Hospital Affiliated to Zhejiang Chinese Medical University, Hangzhou, Zhejiang, China
[9]Key laboratory of cancer prevention and therapy combining traditional Chinese and Western Medicine, Tongde Hospital of Zhejiang Province, Hangzhou, Zhejiang, China
[10]Zhejiang Provincial Key Laboratory of Pancreatic Disease, The First Affiliated Hospital, Zhejiang University School of Medicine, Hangzhou, Zhejiang, China
[11]Institute of Pharmaceutical Biotechnology, Zhejiang University School of Medicine, Hangzhou, Zhejiang, China

X Jun Li @lijun2009

Acknowledgements We would like to thank all the doctors and nurses in the COSSH open cohort study for their selfless dedication and help in completing the study successfully. The authors thank professor Lie Wang (Zhejiang University School of Medicine, Hangzhou, China) for providing helpful comments on revising the manuscript.

Contributors XLia, JinL, QZ, JX, JiaL and BP contributed equally. The study was designed by JunL, DS, XC and YM. XLia, JinL and DS wrote the manuscript. XLia, JinL, PC and HY performed the statistical and bioinformatics analyses. JinL, QZ, JX, JiaL, BP, MH, JJ, WQ, PL, HZ, XZ, JiaC, WH, BL, SM, XW, XLi, JZ, JinC, SL, XF and YL performed the laboratory work. All authors approved the final version of the manuscript. JunL is the guarantor. We used ChatGPT for language polishing.

Funding This study was supported by the Key R&D Program of Zhejiang (2025C02130), the National Natural Science Foundation of China (32330057, 82272426, 82370634), the National Key R&D Program of China (2022YFA1104100, 2022YFC2304800, 2022YFA1104600), the National special support program for high-level personnel recruitment (Ten-thousand Talents Program).

Competing interests The authors declare that they have no conflict of interests.

Patient and public involvement Patients and/or the public were not involved in the design, or conduct, or reporting, or dissemination plans of this research.

Patient consent for publication Not applicable.

Ethics approval The study protocol was approved by the Clinical Research Ethics Committee of the First Affiliated Hospital, Zhejiang University School of Medicine (No. IIT2021-832). Participants gave informed consent to participate in the study before taking part.

Provenance and peer review Not commissioned; externally peer reviewed.

Data availability statement Data are available in a public, open access repository. Data are available upon reasonable request. All data relevant to the study are included in the article or uploaded as supplementary information. All data relevant to the study are included in the article or uploaded as supplementary information. The raw data for scRNA-seq and bulk RNA-seq used in this study have been deposited into the Genome Sequence Archive (https://ngdc.cncb.ac.cn/gsa-human, accession number: HRA007042, HRA007057 and HRA008336).

ORCID iDs
Peng Li https://orcid.org/0000-0003-2215-4871
Jun Li https://orcid.org/0000-0002-7236-8088

REFERENCES

1 Wu T, Li J, Shao L, *et al*. Development of diagnostic criteria and a prognostic score for hepatitis B virus-related acute-on-chronic liver failure. *Gut* 2018;67:2181–91.
2 Weiss E, de la Peña-Ramirez C, Aguilar F, *et al*. Sympathetic nervous activation, mitochondrial dysfunction and outcome in acutely decompensated cirrhosis: the metabolomic prognostic models (CLIF-C MET). *Gut* 2023;72:1581–91.

3 Li P, Liang X, Luo J, *et al*. Predicting the survival benefit of liver transplantation in HBV-related acute-on-chronic liver failure: an observational cohort study. *Lancet Reg Health West Pac* 2023;32:100638.
4 Clària J, Stauber RE, Coenraad MJ, *et al*. Systemic inflammation in decompensated cirrhosis: Characterization and role in acute-on-chronic liver failure. *Hepatology* 2016;64:1249–64.
5 Moreau R, Clària J, Aguilar F, *et al*. Blood metabolomics uncovers inflammation-associated mitochondrial dysfunction as a potential mechanism underlying ACLF. *J Hepatol* 2020;72:688–701.
6 Trebicka J, Fernandez J, Papp M, *et al*. PREDICT identifies precipitating events associated with the clinical course of acutely decompensated cirrhosis. *J Hepatol* 2021;74:1097–108.
7 Li J, Liang X, Jiang J, *et al*. PBMC transcriptomics identifies immune-metabolism disorder during the development of HBV-ACLF. *Gut* 2022;71:163–75.
8 Laleman W, Claria J, Van der Merwe S, *et al*. Systemic Inflammation and Acute-on-Chronic Liver Failure: Too Much, Not Enough. *Can J Gastroenterol Hepatol* 2018;2018:1027152.
9 Jiang Y, Rosborough BR, Chen J, *et al*. Single cell RNA sequencing identifies an early monocyte gene signature in acute respiratory distress syndrome. *JCI Insight* 2020;5:e135678.
10 Sarin SK, Kumar A, Almeida JA, *et al*. Acute-on-chronic liver failure: consensus recommendations of the Asian Pacific Association for the study of the liver (APASL). *Hepatol Int* 2009;3:269–82.
11 Kwok I, Becht E, Xia Y, *et al*. Combinatorial Single-Cell Analyses of Granulocyte-Monocyte Progenitor Heterogeneity Reveals an Early Uni-potent Neutrophil Progenitor. *Immunity* 2020;53:303–18.
12 Ng LG, Ostuni R, Hidalgo A. Heterogeneity of neutrophils. *Nat Rev Immunol* 2019;19:255–65.
13 Schulte-Schrepping J, Reusch N, Paclik D, *et al*. Severe COVID-19 Is Marked by a Dysregulated Myeloid Cell Compartment. *Cell* 2020;182:1419–40.
14 Hassan HM, Cai Q, Liang X, *et al*. Transcriptomics reveals immune-metabolism disorder in acute-on-chronic liver failure in rats. *Life Sci Alliance* 2022;5:e202101189.
15 Bernsmeier C, Triantafyllou E, Brenig R, *et al*. CD14(+) CD15(-) HLA-DR(-) myeloid-derived suppressor cells impair antimicrobial responses in patients with acute-on-chronic liver failure. *Gut* 2018;67:1155–67.
16 Bernsmeier C, Pop OT, Singanayagam A, *et al*. Patients with acute-on-chronic liver failure have increased numbers of regulatory immune cells expressing the receptor tyrosine kinase MERTK. *Gastroenterology* 2015;148:603–15.
17 Weiss E, de la Grange P, Defaye M, *et al*. Characterization of Blood Immune Cells in Patients With Decompensated Cirrhosis Including ACLF. *Front Immunol* 2020;11:619039.
18 Liang X, Li P, Jiang J, *et al*. Transcriptomics unveils immune metabolic disruption and a novel biomarker of mortality in patients with HBV-related acute-on-chronic liver failure. *JHEP Rep* 2023;5:100848.
19 Ren X, Wen W, Fan X, *et al*. COVID-19 immune features revealed by a large-scale single-cell transcriptome atlas. *Cell* 2021;184:1895–913.
20 Shi Y, Yang Y, Hu Y, *et al*. Acute-on-chronic liver failure precipitated by hepatic injury is distinct from that precipitated by extrahepatic insults. *Hepatology* 2015;62:232–42.
21 Cho Y, Bukong TN, Tornai D, *et al*. Neutrophil extracellular traps contribute to liver damage and increase defective low-density neutrophils in alcohol-associated hepatitis. *J Hepatol* 2023;78:28–44.
22 Mookerjee RP, Stadlbauer V, Lidder S, *et al*. Neutrophil dysfunction in alcoholic hepatitis superimposed on cirrhosis is reversible and predicts the outcome. *Hepatology* 2007;46:831–40.
23 Montaldo E, Lusito E, Bianchessi V, *et al*. Cellular and transcriptional dynamics of human neutrophils at steady state and upon stress. *Nat Immunol* 2022;23:1470–83.
24 Chen G, Ren C, Xiao Y, *et al*. Time-resolved single-cell transcriptomics reveals the landscape and dynamics of hepatic cells in sepsis-induced acute liver dysfunction. *JHEP Rep* 2023;5:100718.
25 Peng B, Li H, Liu K, *et al*. Intrahepatic macrophage reprogramming associated with lipid metabolism in hepatitis B virus-related acute-on-chronic liver failure. *J Transl Med* 2023;21:419.
26 Yao J, Ji Y, Liu T, *et al*. Single-Cell RNA Sequencing Shows T-Cell Exhaustion Landscape in the Peripheral Blood of Patients with Hepatitis B Virus-Associated Acute-on-Chronic Liver Failure. *Gut Liver* 2024;18:520–30.
27 Yu X, Yang F, Shen Z, *et al*. BTLA contributes to acute-on-chronic liver failure infection and mortality through CD4+ T-cell exhaustion. *Nat Commun* 2024;15:1835.
28 Meng Y, Ye F, Nie P, *et al*. Immunosuppressive CD10+ALPL+ neutrophils promote resistance to anti-PD-1 therapy in HCC by mediating irreversible exhaustion of T cells. *J Hepatol* 2023;79:1435–49.
29 Sette A, Crotty S. Adaptive immunity to SARS-CoV-2 and COVID-19. *Cell* 2021;184:861–80.
30 Li J, Liang X, You S, *et al*. Development and validation of a new prognostic score for hepatitis B virus-related acute-on-chronic liver failure. *J Hepatol* 2021;75:1104–15.
31 Jalan R, Saliba F, Pavesi M, *et al*. Development and validation of a prognostic score to predict mortality in patients with acute-on-chronic liver failure. *J Hepatol* 2014;61:1038–47.
32 Kawashima K, Andreata F, Beccaria CG, *et al*. Priming and Maintenance of Adaptive Immunity in the Liver. *Annu Rev Immunol* 2024;42:375–99.
33 Hoogeveen RC, Dijkstra S, Bartsch LM, *et al*. Hepatitis B virus-specific CD4 T cell responses differentiate functional cure from chronic surface antigen$^+$ infection. *J Hepatol* 2022;77:1276–86.
34 Andreata F, Laura C, Ravà M, *et al*. Therapeutic potential of co-signaling receptor modulation in hepatitis B. *Cell* 2024;187:4078–94.
35 Garg V, Garg H, Khan A, *et al*. Granulocyte colony-stimulating factor mobilizes CD34(+) cells and improves survival of patients with acute-on-chronic liver failure. *Gastroenterology* 2012;142:e1:505–512..
36 Engelmann C, Herber A, Franke A, *et al*. Granulocyte-colony stimulating factor (G-CSF) to treat acute-on-chronic liver failure: A multicenter randomized trial (GRAFT study). *J Hepatol* 2021;75:1346–54.
37 McGettigan B, Hernandez-Tejero M, Malhi H, *et al*. Immune Dysfunction and Infection Risk in Advanced Liver Disease. *Gastroenterology* 2025;168:1085–100.
38 Leslie J, Mackey JBG, Jamieson T, *et al*. CXCR2 inhibition enables NASH-HCC immunotherapy. *Gut* 2022;71:2093–106.
39 Konishi T, Schuster RM, Goetzman HS, *et al*. Cell-specific regulatory effects of CXCR2 on cholestatic liver injury. *Am J Physiol Gastrointest Liver Physiol* 2019;317:G773–83.
40 Zhang Q, Ma C, Duan Y, *et al*. Gut Microbiome Directs Hepatocytes to Recruit MDSCs and Promote Cholangiocarcinoma. *Cancer Discov* 2021;11:1248–67.
41 Zhou J, Nefedova Y, Lei A, *et al*. Neutrophils and PMN-MDSC: Their biological role and interaction with stromal cells. *Semin Immunol* 2018;35:19–28.
42 Luo J, Li J, Li P, *et al*. Acute-on-chronic liver failure: far to go-a review. *Crit Care* 2023;27:259.
43 Jia L, Xue R, Zhu Y, *et al*. The efficacy and safety of methylprednisolone in hepatitis B virus-related acute-on-chronic liver failure: a prospective multi-center clinical trial. *BMC Med* 2020;18:383.